Published in final edited form as:
J Ultrasound Med. 2009 February ; 28(2): 191–203.

An Intraoperative Brain-shift Monitor Using Shear-mode Transcranial Ultrasound: Preliminary Results

P. Jason White, PhD[1], **Stephen Whalen, BS**[2], **Sai Chun Tang, PhD**[1], **Greg T. Clement, PhD**[1], and **Alexandra J. Golby, MD**[2]

1 *Department of Radiology, Brigham and Women's Hospital, Harvard Medical School, 221 Longwood Avenue, EBRC 521, Boston, MA 02115 USA*

2 *Department of Neurosurgery, Brigham and Women's Hospital, Harvard Medical School, 75 Francis Street, Boston, MA 02115 USA*

Abstract

Objective—Various methods of intraoperative structural monitoring during neurosurgery are used to localize lesions after brain shift and guiding surgically introduced probes such as biopsy needles or stimulation electrodes. With its high temporal resolution, portability, and non-ionizing mode of radiation, ultrasound has potential advantages over other existing imaging modalities for intraoperative monitoring. Yet, sonography is rarely used during neurosurgery largely because of the craniotomy requirement to achieve sufficiently useful signals.

Methods—Prompted by results from recent studies on transcranial ultrasound, a prototype device that aims to use the shear mode of transcranial ultrasound transmission for intraoperative monitoring has been designed, constructed, and tested with 10 human subjects. Magnetic resonance (MR) images were then obtained with the device spatially registered to the MR reference coordinates. Peaks in both the ultrasound and MR signals were identified and analyzed both for spatial localization and signal-to-noise ratio (SNR).

Results—The first results aimed towards validating the prototype device with MRI have demonstrated excellent correlation (n = 38, R^2 = 0.9962) between the structural localization abilities of the two modalities. In addition, the overall SNR of the ultrasound backscatter signals (n = 38, SNR = 25.4±5.2 dB) was statistically equivalent to that of the MR data (n = 38, SNR = 22.5±4.8 dB).

Conclusions—A statistically significant correlation of localized intracranial structures between ITUM and MRI data has been achieved with 10 human subjects. This is the first demonstration and validation of a prototype device incorporating transcranial shear-mode ultrasound towards a clinical monitoring application.

Keywords

ultrasound; neurosurgery; brain shift; transcranial; monitor

1. Introduction

1.1 Intraoperative Ultrasound Monitoring for Neurosurgery

The use of preoperatively acquired images to guide neurosurgery has clear benefits in that it allows surgeons to plan and carry out the initial steps of a surgical procedure with information

Corresponding Author: Phillip Jason White, Department of Radiology, Brigham and Women's Hospital, Harvard Medical School, 221 Longwood Avenue, EBRC 521, Boston, MA 02115, Telephone: (617) 525-7465, Fax: (617) 525-7450, E-mail: white@bwh.harvard.edu.

that is otherwise unobtainable from direct observation of the surgical field. Yet, during the course of surgery, the images progressively become misrepresentations of the actual anatomy due to intraoperative shifts and deformations of the brain.[1–3] The incorporation of an intraoperative tool that can continuously monitor for brain shift and deformation could potentially solve this problem. Recent studies have demonstrated the benefits of intraoperative and perioperative ultrasound, especially as a real-time neuronavigation aid when used in conjunction with preoperative magnetic resonance imaging (MRI) and computed tomographic (CT) images. Intraoperative ultrasound has been used to successfully track brain shift,[4–7] guide needle biopsies,[8] assist in brain mass resections,[8–10] assist in the treatment of vascular malformations,[9–10] guide cystic evacuations,[11] and guide endoscopic procedures.[11] Hyperechoic structures such as biopsy needles and most intraparenchymal mass lesions can be localized in real time, and with sufficiently high spatial resolution. Vascular structures can also be readily and accurately characterized with power Doppler ultrasound, which is useful not only for operations involving vascular malformations, but to identify and track major vessels in the vicinity of targeted lesions.[8,10] Yet, the cumbersome nature of existing devices, lack of an established registration method, and the craniotomy requirement for an acoustic window (when the craniotomy site is used for ultrasound guidance, the surgeon has to stop surgery, position the probe, image, and resume the procedure after the probe has been removed from the surgical field) has limited the applicability of intraoperative ultrasound as a standard tool.[8–11]

A new device, the intraoperative transcranial ultrasound monitor (ITUM), operating transcranially as a real-time monitor during neurosurgical procedures was designed, constructed, and tested in a series of 10 healthy human subjects. The ITUM was developed to have the capability to noninvasively assess, at a high temporal resolution and a sufficient spatial resolution, intracranial deformations of major brain structures. As a low-profile device mounted outside of the surgical field, the ITUM would only require a one-time spatial registration, and would scan continuously without interfering with surgical activities. And since the device scans transcranially, a craniotomy acoustic window would no longer be requisite.

In this preliminary study to validate the ITUM with a “gold standard”, the prototype device was first characterized with benchtop measurements and evaluated for safety. Then, 10 adult healthy subjects were scanned by MRI in conjunction with the spatially-registered ITUM, and the results were analyzed to correlate anatomical structures as defined by both modalities.

1.2 Transcranial ultrasound

Since the first attempts to use ultrasound for medical imaging, scientists have sought a way to image brain tissue with sound waves.[12] Yet, the transmission of ultrasound transcranially to produce backscatter signals with sufficiently useful information has been a severe technical obstacle for the field of neurosonography. Since the skull bone attenuates ultrasound roughly in proportion to the frequency of the signal, there exists a trade-off between the signal-to-noise ratio (SNR) and the resolution of traditional B-mode transcranial ultrasound imagery. In addition, distortions caused by irregularities in the skull’s shape, density, and sound speed collectively contribute toward destroying the integrity of an ultrasound beam.

However, it has been observed that under certain conditions it is possible to propagate ultrasound through the skull with reduced distortion and higher signal amplitudes by using high angles of incidence.[13] Recent studies on shear-mode transcranial ultrasound have suggested that ultrasound beams can be harnessed to image through cranial bone by the intentional induction of a shear-mode ultrasound wave within the skull bone.[13–15] The method prevents skull surface backscatter from interfering with echoes originating from intracranial regions-of-interest and makes diagnostic information easier to analyze than traditional approaches to neurosonography. The method also minimizes refraction of the ultrasound wave

as it passes through bone, making it possible to effectively focus the beam in tissues beyond the bone. In contrast, attempts to use traditional ultrasound are plagued by difficulties resulting from refraction of the ultrasound beam.[16]

Both numeric and experimental investigations indicate that ultrasound transmission enhancement at high angles of incidence is due to the behavior of shear modes induced in the skull bone. When the angle of incidence is beyond Snell's critical angle for the longitudinal pressure wave, ultrasound propagation in the bone becomes purely due to a shear wave. Contrary to the common belief that transcranial shear modes are of negligible application because of distortion[17] and attenuation,[18] it has been demonstrated that the conversion from a longitudinal wave (in the epicranial tissue) to a shear wave (within the skull bone) and back to a longitudinal wave (in the brain parenchyma) does not necessarily produce a highly distorted or small-amplitude wave.[13]

In addition to using shear-mode transcranial propagation, the ITUM incorporates three other application-specific design aspects: (1) a focused ultrasound transducer with a pressure field profile that selectively monitors specific intracranial regions; (2) a lowered effective ultrasound frequency (f_c = 0.96 MHz) to overcome attenuation stemming from the skull bone; and (3) a low ultrasound duty-cycle for time-extended application. This study is the first demonstration of the application of transcranial shear-mode for ultrasound imaging in human subjects.

2. Materials and Methods

2.1 Transducer design and characterization

The ITUM is composed of a lead-zirconate-titanate (PZT) piezoelectric transduction element mounted in a polyvinyl chloride (PVC) housing (Fig. 1). The source element is spherically focused with a 30-mm radius-of-curvature and a 25.4-mm diameter circular aperture, and is electrically poled to operate in the thickness mode (f_0 = 0.96 MHz). The 30-mm radius-of-curvature was selected to specifically focus on the insular cortex/sylvian fissure (ICSF), which typically lies between 20 and 50 mm from the temporal acoustic window. A backing layer consisting of tungsten powder embedded within a polymer matrix is applied to the non-transmitting face of the crystal to increase the radiation bandwidth. A polymer sta ndoff layer at the transmitting aperture is designed to ensure shear angles of incidence between the ultrasound propagation vector and the contact surface. The entire assembly is MRI-compatible and two cylindrical MRI fiduciary markers are mounted on the transducer casing to provide spatial registration with MRI data.

The spatial distribution and spectral content of the ITUM's sonication field was characterized by benchtop measurements. The ITUM was submerged in degassed and deionized water within a rubber-padded tank at room temperature. As it was actuated with a broadband pulser-receiver,[19] the radiated field was raster scanned by a pressure-sensitive polyvinylidene fluoride (PVDF) hydrophone (aperture diameter = 0.2 mm) (Precision Acoustics, Dorchester, UK) mounted to a computer-controlled positioning system (Velmex, Bloomfield, New York, USA). Propagated waveforms were recorded (10,000 points sampled over 100 μs with 4× averaging) at a spatial resolution of 0.5 mm throughout a 20 mm × 60 mm area coplanar with the propagation axis of the ITUM, beginning 20 mm from the transducer aperture. The geometry of the standoff material prohibited the scanning of the field within 20 mm of the transducer aperture.

To determine the spectral properties of the ITUM's performance, Fourier analysis was performed with Matlab (Mathworks, Natick, Massachusetts, USA) on the recorded waveform at the focus of the radiated field. The subsequent reconstruction of the spatial distribution of the ultrasound intensity was based on the results of the spectral analysis.

2.2 Transcranial shear-mode backscatter signal analysis

Previous studies have established the enhancement of ultrasound propagation through the skull at high angles of incidence using a one-way through-transmission method.[13] For this study, measurements were performed to determine if similar results could be achieved using the ITUM under a pulse-receive backscatter analysis scenario.

The ITUM was again submerged in degassed and deionized water within a rubber-padded tank at room temperature (Fig. 2). The actuating pulser-receiver in this and all subsequent experiments was a customized system designed specifically for transcranial ultrasound applications.[19] The system delivered controlled 3-cycle high-voltage pulses at a frequency of 1.0 MHz with a pulse-repetition-frequency of 6 Hz, and then detected and amplified the backscattered echoes received at the transducer face. A spherical steel backscatter target (diameter = 3.1 mm) was mounted via a thin rigid steel needle onto a computer-controlled positioning system (Velmex, Bloomfield, New York, USA) and positioned within the propagation field of the ITUM such that the needle mount was parallel to the propagation axis (Fig. 2).

Then, an ex vivo human skull fixed in 10% buffered formalin (formalin-fixed human skulls have been shown to have the same ultrasound characteristics as non-fixed skull bone)[20] was mounted to a rotary positioning system and positioned between the ITUM and the steel target such that ultrasound was propagated through the thickness dimension of the left temporal bone (approximately 30 mm superior to the external auditory meatus). The right half of the skull was excised for this experiment. The skull was positioned such that the angle of incidence could be varied from 0° to 35°; the rotation was such that increasing the angle of incidence directed the ultrasound beam path more towards the posterior of the cranial vault (Fig. 2). A 50-mm distance between the ITUM and the skull was geometrically necessary to achieve these angles of incidence. For each angle of incidence between 0° to 35°, in step sizes of 5°, a 20 mm × 20 mm scan (scan resolution of 0.5 mm) of the backscatter field was performed by raster scanning the steel target and recording the backscattered signal as received by the ITUM, pulser-receiver, and oscilloscope system (Tektronix, Beaverton, Oregon, USA) at each grid location (Fig. 2). The recorded waveforms were then analyzed with Matlab to yield backscatter field reconstructions.

2.3 Validation with human subjects and MRI

Ten healthy adult subjects were recruited for measurements to validate ITUM results against MRI data. The Partner's Institutional Review Board approved the protocol and all subjects gave written informed consent. Safety studies (benchtop and animal) had been performed to assess thermal effects, mechanical index, and current leakage associated with the ITUM. The system delivered controlled 3-cycle high-voltage pulses at a frequency of 1.0 MHz with a pulse-repetition-frequency of 6 Hz, and then detected and amplified backscattered echoes received at the transducer face. These excitation parameters (3-μs pulse trains at 6 Hz gives a duty cycle of less than 0.002%) were designed to yield a sufficiently low time-averaged power for extended application in the operating room. Even under the worst-case scenario of perfect energy absorption in the tissue, the applied time-averaged power of approximately 1.4 mW over 1 s would raise a 1-g tissue mass (specific heat ~ 3500 J/kg·°C) by 0.0004°C. The peak rarefaction pressure for the ITUM was measured to be on the order of 0.1 MPa in water.

The ITUM was mounted onto an MRI-compatible adjustable arm, which was then attached to an MRI head coil. Each subject was positioned in a head-first supine position on the scanner bed, and the ITUM was placed in contact against the right temple (approximately 50 mm posterior to the lateral canthus of the eye), aligned to project in a posteromedial trajectory

within the cranial vault (Fig. 3). Ultrasound gel (Parker, Fairfield, New Jersey, USA) was applied on both the scalp and the ITUM contact surface to ensure adequate ultrasound coupling.

The ITUM was then actuated with the parameters as specified above, and a time trace of the received backscattered signal was recorded (10,000 points sampled over 200 μs with 8× averaging). The same sequence was acquired without the subject (ITUM radiating into air) to be used as a baseline time trace. The subjects were then placed in the scanner (3.0-Tesla MRI scanner, General Electric Healthcare, Milwaukee, Wisconsin, USA), and a series of MRI scans were performed with the ITUM in place (but not actuated). First, a three-dimensional fast spoiled gradient-echo (3D FSPGR, TR = 7.5 ms, TE = 3.0 ms, NEX 1, FOV = 25.6 cm × 25.6 cm, sl ice thickness = 1.0 mm) was performed, taking care to include the ITUM fiduciary markers within the field-of-view. The images from this scan were used to plan the second scan, which was a spin-echo T1-weighted coronosagittal oblique scan (SE T1, TR = 650 ms, TE = 10 ms, NEX 0.75, FOV variable, slice thickness = 4.0 mm) that was aligned to be coplanar with the propagation axis of the ITUM, as identified by the fiduciary markers (Fig. 3).

2.4 Signal processing and data analysis

Statistical analysis was performed on the two sets of data (ITUM and MRI) to establish a correlation between the observed locations of intracranial anatomical structures. First, the path of ultrasound propagation was identified in the MRI oblique scan, and the pixel values along this path were extracted for analysis. To make a meaningful comparison between the MRI pixel-value and the ultrasound backscatter vector, the absolute value of the first derivative with respect to the path was performed on the MRI data, i.e.,

$$\mathrm{MR}=\left|\frac{d}{dx}(PV)\right|, \tag{1}$$

where PV is the pixel value and x is the path of ultrasound propagation. The rationale being that a change in structure composition (an anatomical boundary) is related to a change in the characteristic acoustic impedance, which is the source of a backscattered signal. A local peak in this value should then correspond to a local peak in backscattered ultrasound data.

Next, the recorded ITUM backscatter signal was subtracted from the recorded baseline time-trace, and the time segment of interest was extracted for comparison with the processed MRI data. Sound speeds of 1562 m/s for the brain parenchyma[21] and 1500 m/s for the skull bone shear-mode[14] were used to accurately convert the time sequences into propagation distances. The ITUM signal was processed according to

$$\mathrm{US}_{\mathrm{NA}}=H\left\{\left[I(t)-I_B(t)\right]*\left[e^{-t^2/0.2}\sin(2\pi t)\right]\right\}, \tag{2}$$

where $I(t)$ is the ITUM backscatter data, $I_B(t)$ is the ITUM baseline data, t is the time vector corresponding to the recorded data, $*$ represents a cross-correlation performed in Fourier space, H is the Hilbert transform, and $\mathrm{US}_{\mathrm{NA}}$ represents the non-attenuated processed ultrasound signal. The cross-correlation of a Gaussian-enveloped sinusoid with the backscattered signal was performed in accordance with a method previously developed for improving ultrasound resolution and signal strength through highly attenuating media.[22] A propagation-distance-dependent attenuation factor was also applied to the resulting backscatter A-line signal to compensate for signal loss due to attenuation within the brain. This was done according to

$$\mathrm{US}=\mathrm{US}_{\mathrm{NA}}\cdot e^{\alpha f d}, \tag{3}$$

where α is the attenuation coefficient (0.87 dB/cm/MHz),[21] f is the ultrasound frequency (0.96 MHz), d is the propagation distance, and $\mathrm{US}_{\mathrm{NA}}$ is the non-attenuated result from Eq. (2) ("US" represents the processed ultrasound data both here and in the figures).

Signal peaks in both the MR and US data were identified and analyzed for correlation in the localization of intracranial structures. To exclude data that do not originate from intracranial structures, signal peaks between 0 mm and 20 mm were not included in the analysis. During data acquisition, a slight oscillation of approximately 1 Hz in signal arrival time could be observed for each subject, but only for signals originating from intracranial structures. This oscillatory motion was most likely due to cardiac-induced pulsatile motion, and so was also used qualitatively to confirm that the signal was of intracranial origin.

To compare the observed distance-from-device from ITUM backscatter signal peaks (US) and MRI pixel intensity gradients (MR), linear regression analysis was used (i.e., calculation of slope, *y*-intercept, and correlation coefficient). A paired Student *t*-test confirmed zero bias between comparisons. The Bland-Altman technique[23] was also used to evaluate the agreement between the measurements, with the limits of agreement defined as the mean difference ± 1.96 standard deviations. Specific to the design of this study was the observation and localization of the insular cortex/sylvian fissure (ICSF) (Fig. 3), this being a prominent hyperechoic structure due to its extensive cerebrospinal fluid (CSF)-cortex structural boundaries. The ICSF was clearly identifiable in all MRI scans by visual inspection. A signal peak from each of the ITUM and the MRI series was identified as originating from the ICSF, and a separate statistical analysis was performed on this set of measurements.

Finally, SNR calculations and statistical analyses (subject mean, subject standard deviation, overall mean, and overall standard deviation) were performed independently on the series of ITUM and MRI data. The SNR was defined as

$$\mathrm{SNR(dB)}=20\log_{10}\left(\frac{A_S}{A_N}\right), \tag{4}$$

where A_S is the signal amplitude and A_N is the mean noise amplitude. The mean noise amplitude, A_N, was obtained by selecting a series of temporo-spatial points beyond the signal and applying the formula

$$A_N=\frac{1}{n}\sum_{1}^{n}\left|A_n-\bar{A}_n\right|, \tag{5}$$

Where n is the number of points sampled, A_n is the value of the point n as obtained by Eqs. 1–3, and $\bar{A}$ is the mean values of all n points. The overall statistical analyses were also independently performed on the SNR as measured from signals arising from the ICSF.

3. Results

3.1 Transducer design and characterization

The radiated pressure field of the prototype ITUM was spatially scanned. Fourier analysis of the recorded waveform at the focus of the radiated pressure field revealed a peak at 0.96 MHz with a −3-dB bandwidth of 260 kHz (Fig. 4). The intensity field reconstruction was then performed at this frequency, yielding a spatial full-width-at-half-maximum (FWHM) intensity profile of 4.8 mm (orthogonal to the propagation vector) at a distance of 30 mm from the aperture (Fig. 4). A slight standing-wave-effect undulation in the intensity along the propagation direction was observed in the focal area of the field. This pattern was most likely due to wave interaction with the ultrasound signal reflected from the hydrophone mount.

3.2 Transcranial shear-mode backscatter signal analysis

The results from the transcranial backscatter field scans corroborated earlier studies[13–14] on the enhancement of ultrasound transmission through the skull bone at high angles of incidence. In the present study, the reduced distortion of the shear mode was made evident by the detection of a backscattered signal from a point-like target. It was observed that the backscattered signal from a steel sphere as transmitted and received by the ITUM decreased in amplitude as an intervening ex vivo skull was rotated to increase the ultrasound beam's angle of incidence (Fig. 5). This reduction in backscattered amplitude continued as the angle of incidence was increase to approximately 30°, at which point the signal was observed to increase in amplitude with increasing angle of incidence. The backscattered amplitude continued to increase until the geometry of the experimental setup would not allow further rotation (θ_i = 35°). At this angle of incidence, the peak intensity was 84% of the original peak intensity at normal incidence (Fig. 6). At its lowest (θ_i = 20°), the backscattered peak intensity was 4% of the original peak intensity at normal incidence.

It was also observed that beyond a critical angle of incidence (approximately 30°), the backscattered signal from the target became less distorted and more clearly isolated from spurious signals. A double backscattered signal as received by the ITUM from the target was evident when the skull was aligned at normal incidence (Fig. 5). As the angle of incidence was increased beyond 10°, the signal that arrived at an earlier time (approximately 165 μs) disappeared, leaving only a single signal (arriving at approximately 177 μs), which was then enhanced as the angle of incidence was increased beyond 30°. A qualitative assessment of the scanned backscattered intensity fields (Fig. 6) revealed an incident-angle-dependent increase in distortion of the spatial distribution of backscattered intensity as θ_i was increased from 0° to 25°. The scanned fields for θ_i =30° and θ_i =35° were markedly less-distorted than those at θ_i =20° and θ_i =25°, and somewhat less distorted than the angles of incidence between 0° and 15°.

3.3 Validation with human subjects and MRI

The ICSF was identifiable in both the MRI data and the ITUM data for each of the 10 healthy adult subjects (Fig. 7). In addition to the ICSF, 28 other structures (e.g., outer cortex, superior temporal sulcus, and later ventricle) were identified to be correlative for both series of data, from as many as seven intracranial structures for one subject to only one structure (the ICSF) for one subject (Fig. 8). Most of these structures were in the vicinity of the ICSF (between 20 mm and 60 mm from the scalp), but 5 backscattered signals originating from structures beyond 80 mm were identified on the MR image as the margins of the ipsilateral lateral ventricles. Statistical analysis was performed for both the complete set of signals arising from all intracranial structures (n = 38) and those signals arising from the ICSF (n = 10).

Linear regression analysis confirmed a high level of correlation between MRI localization and the localization of the same structures with the ITUM (slope = 1.02, *y*-intercept = −0.06, and R^2 = 0.9962 for all structures; slope = 1.05, *y*-intercept = −0.20, and R^2 = 0.9922 for ICSF). Confirmation of a significant correlation between the two series of measurements was also achieved with the Bland-Altman technique of analysis, using the mean of the two measured values as the independent variable and the difference between the two measured values as the dependent variable. For the case of all identified structures, only two measurements fell beyond ±1.96 standard deviations; for the case of the ICSF measurements, no data points fell outside ±1.96 standard deviations.

The SNR for each signal peak was also measured for both the MRI data and the ITUM signals in two categories (Fig. 9): all identifiable structures (*n* = 38) and ICSF only (*n* = 10). Overall, the SNR levels of the ITUM signals were statistically equivalent to those of the MRI signals. The mean SNR for the ITUM backscattered signals was 25.4±5.2 dB for all structures and 28.5 ±8.2 dB for the ICSF. For the MRI signal peaks, the mean SNR was 22.5±4.8 dB for all structures and 25.3±5.6 dB for the ICSF. As would be expected, the mean SNR values for signals arising from the ICSF were higher than the corresponding mean SNR values when all other structures were considered. The lowest and highest SNR values obtained by MRI were 14.8 dB and 36.0 dB, respectively. The lowest and highest SNR values obtained by the ITUM were 14.4 dB and 38.6 dB, respectively.

4. Discussion

The clinical impetus for intraoperative navigational aid stems from the need to visualize anatomical structural changes and surgical tool placements that are not readily observable directly from the operative field. These include the localization of lesions after brain shift,[24] the identification of acute iatrogenic pathologies such as intracranial hemorrhage,[25] and the guidance of surgically introduced probes such as biopsy needles[26] or stimulation electrodes.[27]

While MRI is effective in the spatial localization of such targets, it lacks efficacy as a real-time monitor during surgery because real-time scanning cannot take place during surgical activities (e.g., dural opening, lesion resection, and biopsy). The typical protocol for MRI-guided surgery requires the cessation of surgical procedures and the clearing of metallic tools from the surgical field to minimize image artifacts. The time added to the overall duration of a procedure and to the time during which a patient is under general anesthesia increases the chance of surgical complications. Also, standard MRI pulse sequences have insufficient time resolutions to monitor acute status changes during a procedure. Emergent surgical complications that require immediate attention (e.g., acute hemorrhage, aneurysm rupture, and excessive brain shift) occur on a time scale of seconds, while MRI can give feedback only at a temporal resolution of minutes. Due to these inherent MRI deficiencies, surgeons are required to weigh the benefit of scanning time with diagnostic potential before ordering an intraoperative scan. In addition, intraoperative MRI is very resource intensive and its availability is limited to a few dedicated centers. These shortcomings in MRI-guided neurosurgery prompted the design and investigation of the ITUM, which has the potential to be deployed in any operating room for intraoperative monitoring.

The discovery that a focused ultrasound beam, traveling as a shear wave through the skull, may emerge less distorted than a longitudinal one[13–14] became a key design aspect for incorporation into the ITUM. In contrast with shear wave imaging in soft tissue, the ITUM was designed to incorporate a traditional compression-wave backscatter imaging modality with an interposed shear conversion within the osseous tissue of the skull bone. By directing a longitudinal wave onto the skull surface at angles beyond 30°, a generated shear wave travels

through the thickness dimension of the skull bone in a direction nearly identical to the initial direction of propagation. When the shear wave reaches the interior surface of the skull, the energy is converted back into a longitudinal wave. Backscatter signals from intracranial structures undergo the same mode conversion as they travel along the same path back to the transducer.

This backscatter detection mode of operation was shown to be effective by benchtop experiments (cf. 3.2). At near-normal angles of ultrasound incidence, a double backscattered signal originating from the same target was observed, most likely due to the combined effects of modal bifurcation at the skull interfaces. With a longitudinal mode phase speed of approximately 2800 m/s[14,20] and a shear mode phase speed of approximately 1500 m/s,[14] the actuation of both modes at the skull surface (the generation of only a longitudinal with no shear component within an ex vivo skull is not possible in an experimental setting) resulted in two detectable signals with different arrival times. The double backscatter signals obscured and distorted the definition of the single point-like target. The signal stemming from the longitudinal mode actuation decreased as the ultrasound incident angle at the skull surface was increased. After the critical angle for longitudinal transmission was reached, as defined by

$$\theta_c = \sin^{-1}\left(\frac{c_1}{c_2}\right), \tag{6}$$

where c_1 is the sound speed of the first medium and c_2 is the longitudinal sound speed of the second medium (in the case of an ex vivo human skull in water, $c_1 \approx 1500$ m/s and $c_2 \approx 2800$ m/s, and so $\theta_i \approx 32°$), it was observed that only one backscatter signal remained. This result gave strong support to the incorporation of shear mode transcranial ultrasound into the design of the ITUM. Together with the lowered frequency of operation, the transcranial shear mode of operation was a significant contributor to the high SNR and the precision of localization exhibited by the ITUM.

The high level of correlation between the MRI and ITUM localization of intracranial structures ($R^2 = 0.9962$) was demonstrated predominantly by backscattered signals within the spatial range of 2–6 cm from the ITUM aperture. Since this study focused on signals originating from the ICSF, the observation of five signals emanating from the margins of the lateral ventricles (beyond 8 cm from the aperture of the ITUM) was incidental. The inclusion of these data points in the overall analysis may have reduced the correlation results (this is most notable in the Bland-Altman plot) or the SNR values, but a substantially high correlation was maintained nonetheless and no significant difference was evident in the SNR analysis. Future studies are being designed that will focus on localization and motion tracking of the lateral ventricles and other deeper-set structures, including the midline falx, basal ganglia, and brainstem structures. It is anticipated that subarachnoid hemorrhage (SAH) could also have a significant impact on backscatter distortion and SNR, and as such, may be investigated for use as a monitoring method for intraoperative SAH.

Acknowledgements

Dr. Clement is an original inventor on patent # 7175599. He has no current financial interest in this intellectual property. This work was funded by NIH P01CA067165, NIH 1U41RR019703-01A2, and NIH R21EB004353.

References

1. Dorward NL, Alberti O, Velani B, et al. Postimaging brain distortion: Magnitude, correlates, and impact on neuronavigation. J Neurosurg 1998;88:656–662. [PubMed: 9525711]

2. Hill DL, Maurer CR, Maciunas RJ, et al. Measurement of intraoperative brain surface deformation under a craniotomy. Neurosurgery 1998;43:514–528. [PubMed: 9733307]
3. Roberts DW, Hartov A, Kennedy FE, et al. Intraoperative brain shift and deformation: A quantitative analysis of cortical displacement in 28 cases. Neurosurgery 1998;43:749–760. [PubMed: 9766300]
4. Comeau RM, Sadikot AF, Fenster A, et al. Intraoperative ultrasound for guidance and tissue shift correction in image-guided neurosurgery. Med Phys 2000;27:787–800. [PubMed: 10798702]
5. Coenen VA, Krings T, Weidemann J, et al. Sequential visualization of brain and fiber tract deformation during intracranial surgery with three-dimensional ultrasound: an approach to evaluate the effect of brain shift. Neurosurgery 2005;56:133–139. [PubMed: 15799801]
6. Lindner D, Trantakis C, Renner C, et al. Application of intraoperative 3D ultrasound during navigated tumor resection. Minim Invas Neurosurg 2006;49:197–202.
7. Letteboer MMJ, Willems PWA, Viergever MA, et al. Brain shift estimation in image-guided neurosurgery using 3-D ultrasound. IEEE Trans Biom Eng 2005;52:268–276.
8. Sosna J, Barth MM, Kruskal JB, et al. Intraoperative sonography for neurosurgery. J Ultrasound Med 2005;24:1671–1682. [PubMed: 16301724]
9. Tirakotai W, Miller D, Heinze S, et al. A novel platform for image-guided ultrasound. Neurosurgery 2006;58:710–718. [PubMed: 16575335]
10. Unsgaard G, Rygh OM, Selbekk T, et al. Intra-operative 3D ultrasound in neurosurgery. Acta Neurochirurgica 2006;148:235–253. [PubMed: 16362178]
11. Strowitzki M, Kiefer M, Steudel W. A new method of ultrasonic guidance of neuroendoscopic procedures. J Neurosurg 2002;96:628–632. [PubMed: 11883854]
12. Dussik KT. On the possibility of using ultrasound waves as a diagnostic aid. Neurol Psychiat 1942;174:153–168.
13. Clement GT, White PJ, Hynynen K. Enhanced ultrasound transmission through the human skull using shear mode conversion. J Acoust Soc Am 2004;115:1356–1364. [PubMed: 15058357]
14. White PJ, Clement GT, Hynynen K. Longitudinal and shear mode ultrasound propagation in human skull bone. Ultrasound in Med Biol 2006;32:1085–1096. [PubMed: 16829322]
15. Pichardo S, Hynynen K. Treatment of near-skull brain tissue with a focused device using shear-mode conversion: a numerical study. Phys Med Biol 2007;52:7313–7332. [PubMed: 18065841]
16. White DN, Clark JM, Chesebrough JN, et al. Effect of skull in degrading the display of echoencephalographic B and C scans. J Acoust Soc Am 1968;44:1339–1345. [PubMed: 5699038]
17. Clement GT, Sun J, Hynynen K. The role of internal reflection in transskull phase distortion. Ultrasonics 2001;39:109–113. [PubMed: 11270628]
18. Hayner M, Hynynen K. Numerical analysis of ultrasonic transmission and absorption of oblique plane waves through the human skull. J Acoust Soc Am 2001;110:3319–3330. [PubMed: 11785832]
19. Tang SC, Clement GT, Hynynen K. A computer-controlled ultrasound pulser-receiver system for transkull fluid detection using a shear wave transmission technique. IEEE Trans Ultrason Ferroelect Freq Contr 2007;54:1772–1783.
20. Fry FJ, Barger JE. Acoustical properties of the human skull. J Acoust Soc Am 1978;63:1576–1590. [PubMed: 690336]
21. Kremkau FW, Barnes RW, McGraw CP. Ultrasonic attenuation and propagation speed in normal human brain. J Acoust Soc Am 1981;70:29–38.
22. Clement GT. Spectral image reconstruction for transcranial ultrasound measurement. Phys Med Biol 2005;50:5557–5571. [PubMed: 16306652]
23. Bland JM, Altman DG. Statistical methods for assessing agreement between two methods of clinical measurement. Lancet 1986;1:307–310. [PubMed: 2868172]
24. Nabavi A, Black PM, Gering DT, et al. Serial intraoperative magnetic resonance imaging of brain shift. Neurosurgery 2001;48:787–797. [PubMed: 11322439]
25. Morandi X, Haegelena C, Henauxa PL, et al. Brain shift is central to the pathogenesis of intracerebral haemorrage remote from the site of the initial neurosurgical procedure. Med Hypotheses 2006;67:856–859. [PubMed: 16750308]
26. Rubin JM, Dohrmann GJ. Intraoperative neurosurgical ultrasound in the localization and characterization of intracranial masses. Radiology 1983;148:519–524. [PubMed: 6867352]

27. Moringlade JR, Fuss G, Becker GB. Peroperative transcranial sonography for electrode placement into the targeted subthalamic nucleus of patients with Parkinson disease: technical note. Surgical Neurology 2005;63:66–69. [PubMed: 15639532]

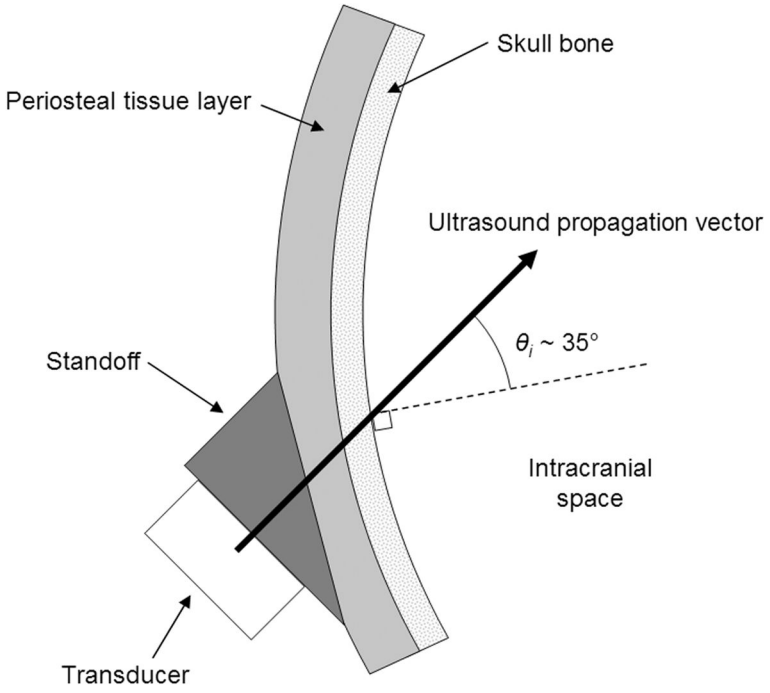

Figure 1.
A schematic of the prototype intraoperative transcranial ultrasound monitor (ITUM) positioned against the skull.

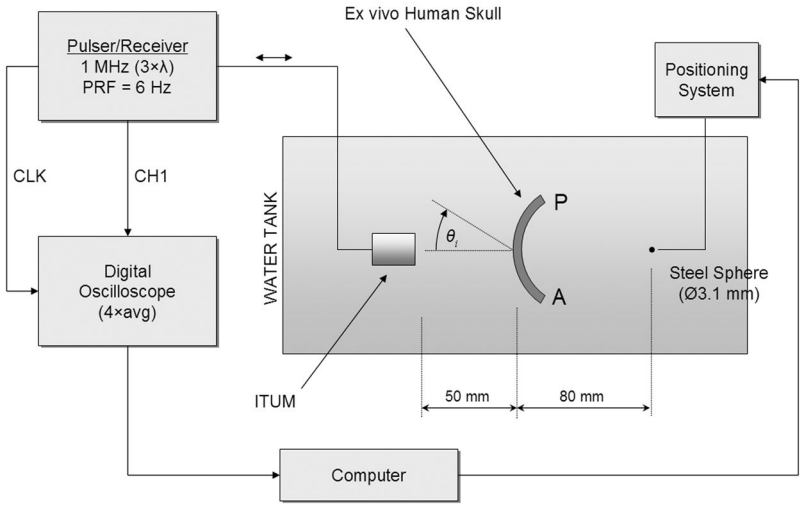

Figure 2.

A schematic of the experimental setup for investigating the effects of the angle of incidence on transcranial backscatter detection. In this view, the ultrasound incident angle ($\boldsymbol{\theta_i}$) was increased by rotating the skull in a clockwise fashion, with the posterior aspect of the skull (**P**) moving towards the right of the figure, and the anterior aspect of the skull (**A**) moving towards the left of the figure. The figure is not drawn to scale.

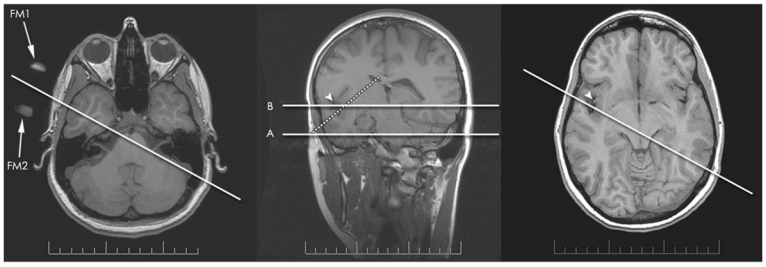

Figure 3.

A diagram demonstrating the registration of MR images with the ITUM in a healthy human subject. An axial section (*left*, 3D FSPGR, TR = 7.5 ms, TE = 3.0 ms, FOV = 25.6 cm × 25.6 cm, slice thickness = 1.0 mm) containing the fiduciary markers (**FM1** and **FM2**) of the ITUM was used to prescribe the oblique section (*center*, SE T1, TR = 650 ms, TE = 10 ms, FOV = 24.0 cm × 24.0 cm, slide thickness = 3.0 mm) that was used for signal analysis. A second axial slice demonstrates the location of the insular cortex/sylvian fissure (*right*, 3D FSPGR, TR = 7.5 ms, TE = 3.0 ms, FOV = 25.6 cm × 25.6 cm, slice thickness = 1.0 mm). The solid lines indicate the corresponding slices for both images (in the *center* diagram, line **A** corresponds to the image on the *left*, line **B** corresponds to the image on the *right*), the dotted line indicates the ultrasound propagation direction, and the arrowheads indicate the insular cortex/sylvian fissure (ICSF).

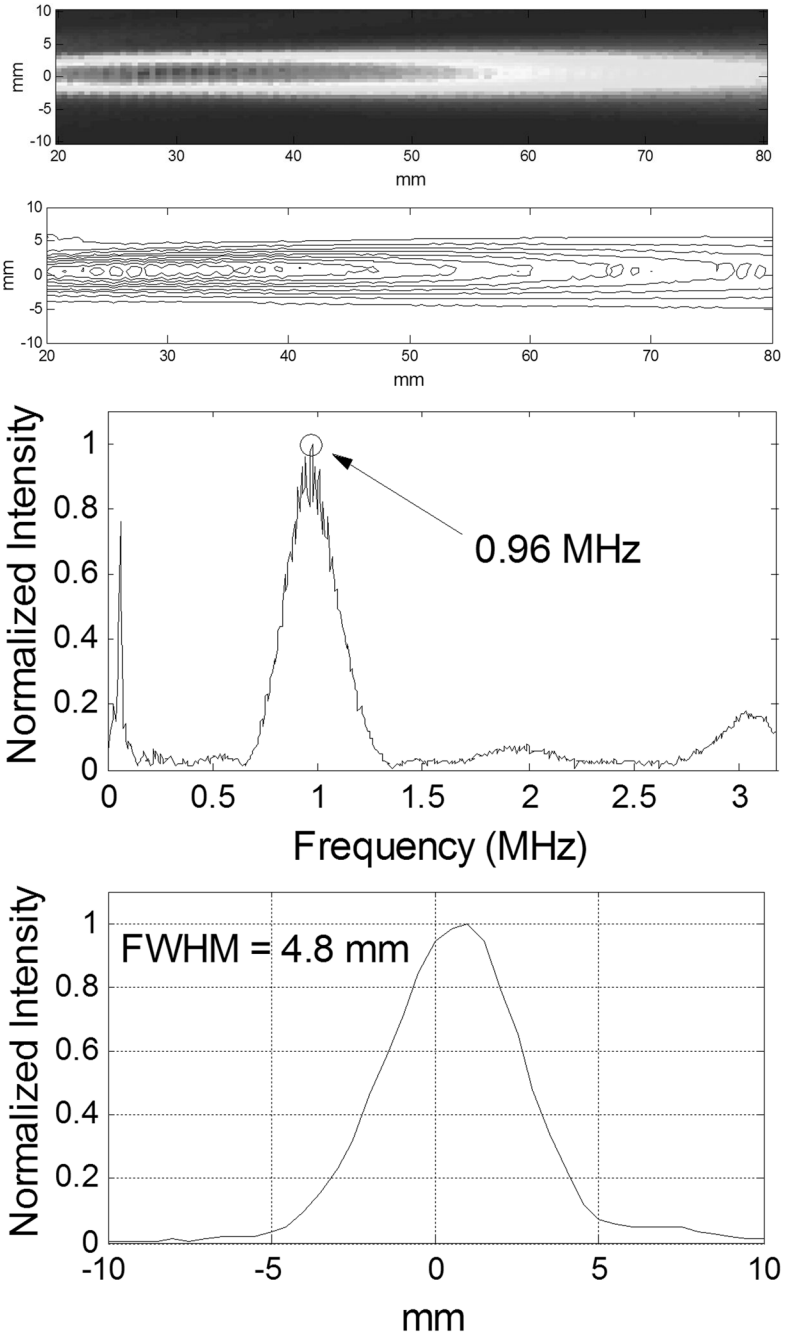

Figure 4.

Experimental results from the benchtop characterization of the prototype ITUM: (**A**) the reconstructed intensity map of the ITUM's radiation pattern, (**B**) the same intensity radiation profile as depicted with 10% contour lines, (**C**) the spectral impulse response of the ITUM (circle marks the peak at 0.96 MHz), and (**D**) the cross-section of the spatial intensity profile at 30 mm from the transducer aperture.

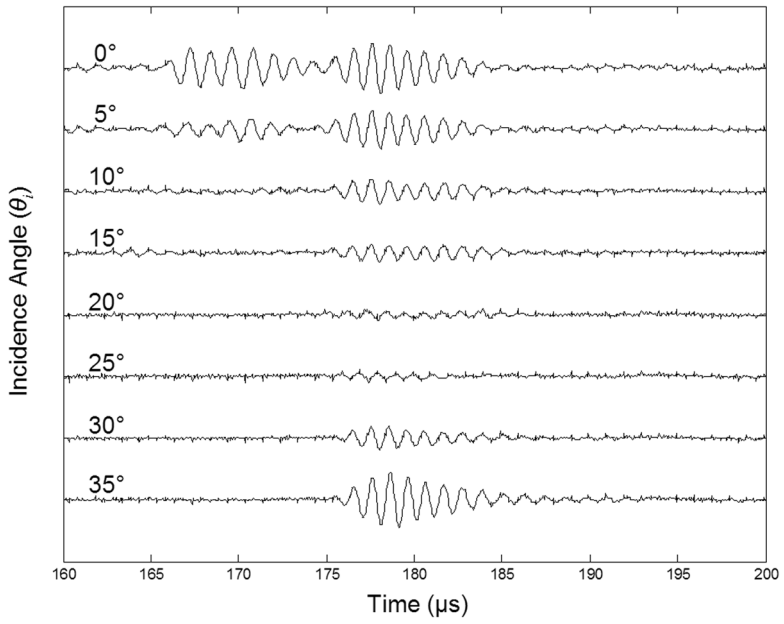

Figure 5.
Time-windowed backscatter signals from a 3.1-mm-diameter steel sphere as received by the ITUM after transcranial signal propagation. Results from a sequence of 8 ultrasound angles of incidence, ranging from normal (0°) to 35°, are shown.

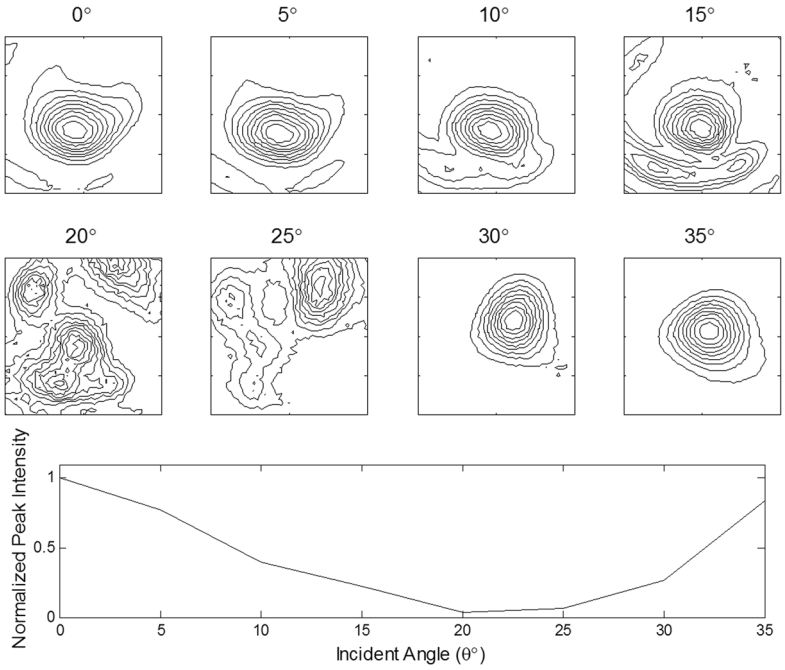

Figure 6.

Spatial distributions of backscatter intensities from a 3.1-mm-diameter steel sphere as received by the ITUM after transcranial signal propagation. (**A**) Each plot represents the backscatter intensity measured on a 20 mm × 20 mm grid lying orthogonal to the propagation axis of the ITUM (10% contour lines, scanning resolution of 0.5 mm). The plots range from a normal incident angle (0°) (*upper-left*) to an incident angle of 35° (*lower-right*). (**B**) A plot of the peak measured backscattered intensity (normalized) for each of the fields in (**A**).

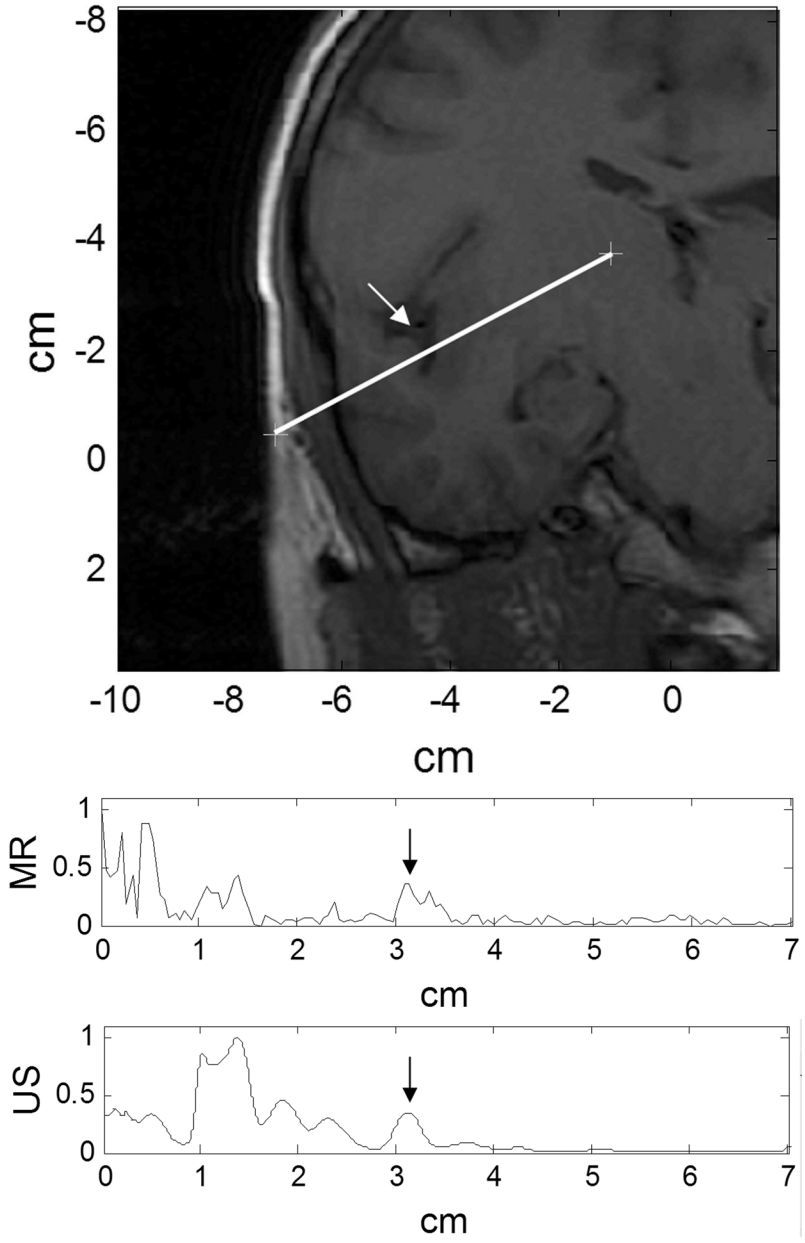

Figure 7.

(**A**) Detail of an oblique MRI scan (SE T1, TR = 650 ms, TE = 10 ms, FOV = 12.0 cm × 12.0 cm, slice thickness = 3.0 mm) that has been registered with the ITUM's signal path (solid line) through the ICSF (arrow). (**B**) The absolute value of the MRI pixel-intensity-gradient corresponding to the ITUM signal path and (**C**) the processed ITUM backscatter signal. Signal peaks corresponding to the ICSF can be identified in both (**B**) and (**C**) at approximately 3.1 cm (arrows).

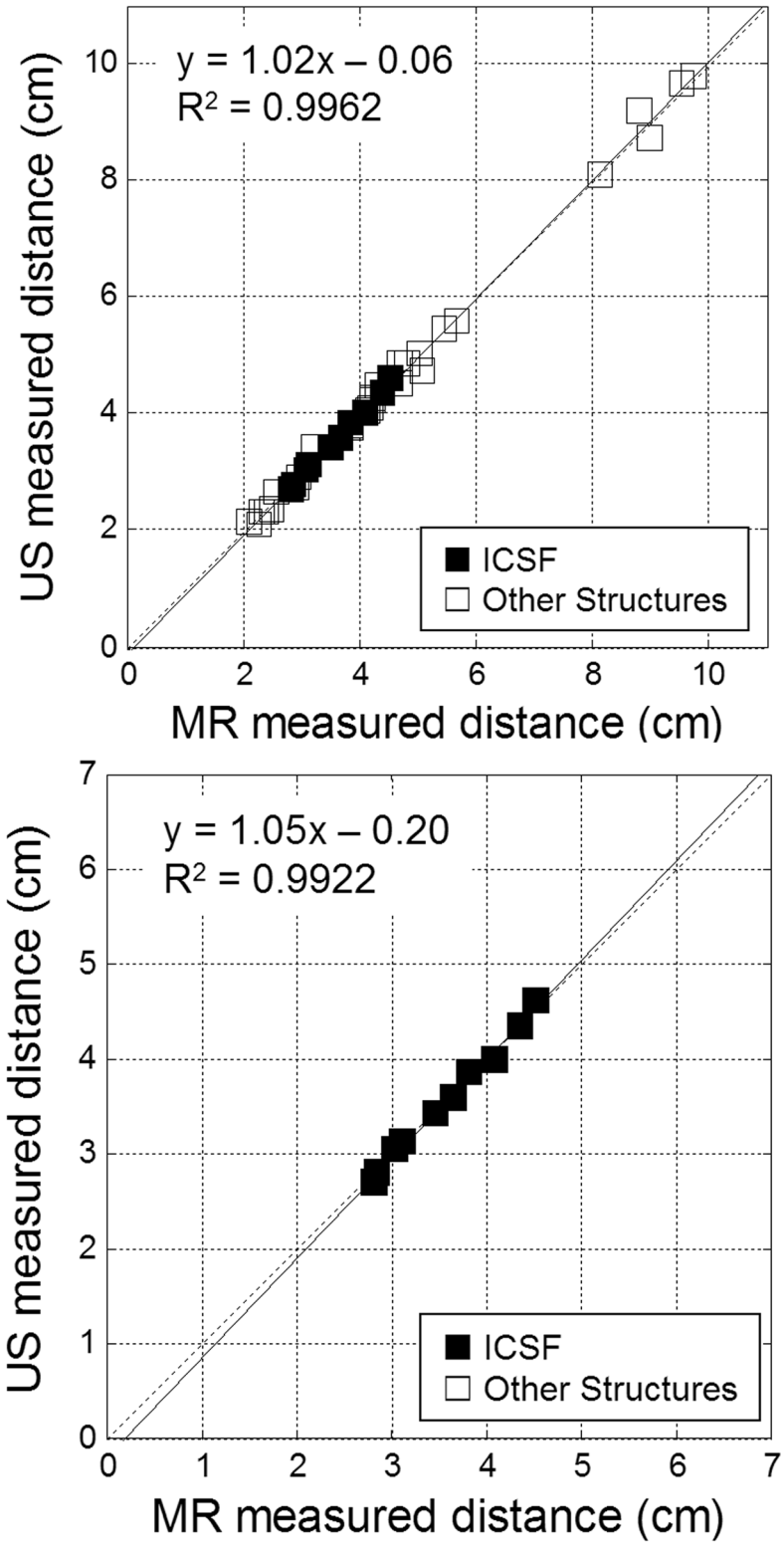

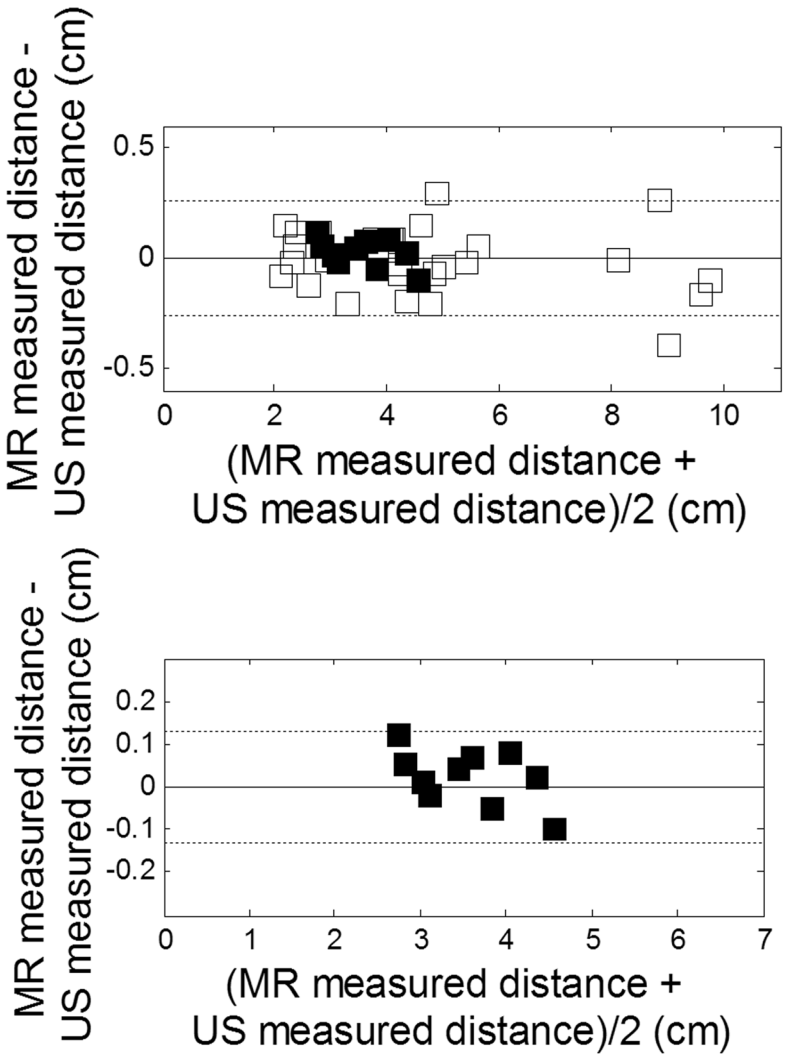

Figure 8.

Results of the statistical analysis to validate the ability of the ITUM to localize intracranial structures against the "gold standard" of MR imaging. (**A**) The location of intracranial structures as measured by the ITUM is plotted against the same measurement performed by MRI. (**B**) Same as (**A**), but with analysis performed on only those signal peaks originating from the ICSF. In (**A**) and (**B**), solid line = linear regression, dotted line = perfect correlation. (**C**) The results of a Bland-Altman analysis comparing the mean of the two series of measurements (MR and US) with the difference between the same measurements. (**D**) Same as (**C**), but with Bland-Altman analysis performed on only those signal peaks originating from the ICSF. In (**C**) and (**D**), solid line = perfect correlation, dotted line = ±1.96 standard deviations. For (**A**, **B**, **C**, and **D**), black squares = signal peaks originating from the ICSF, white squares = signal peaks originating from all other intracranial structures.

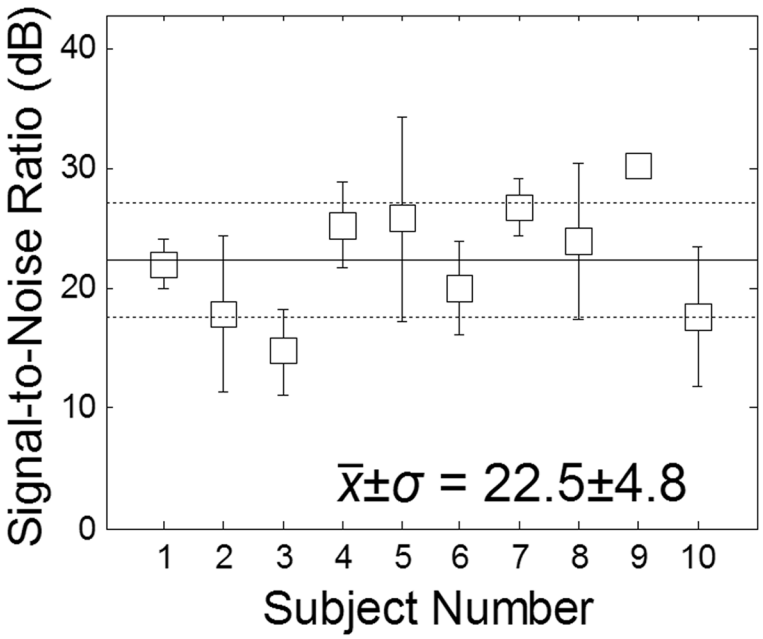

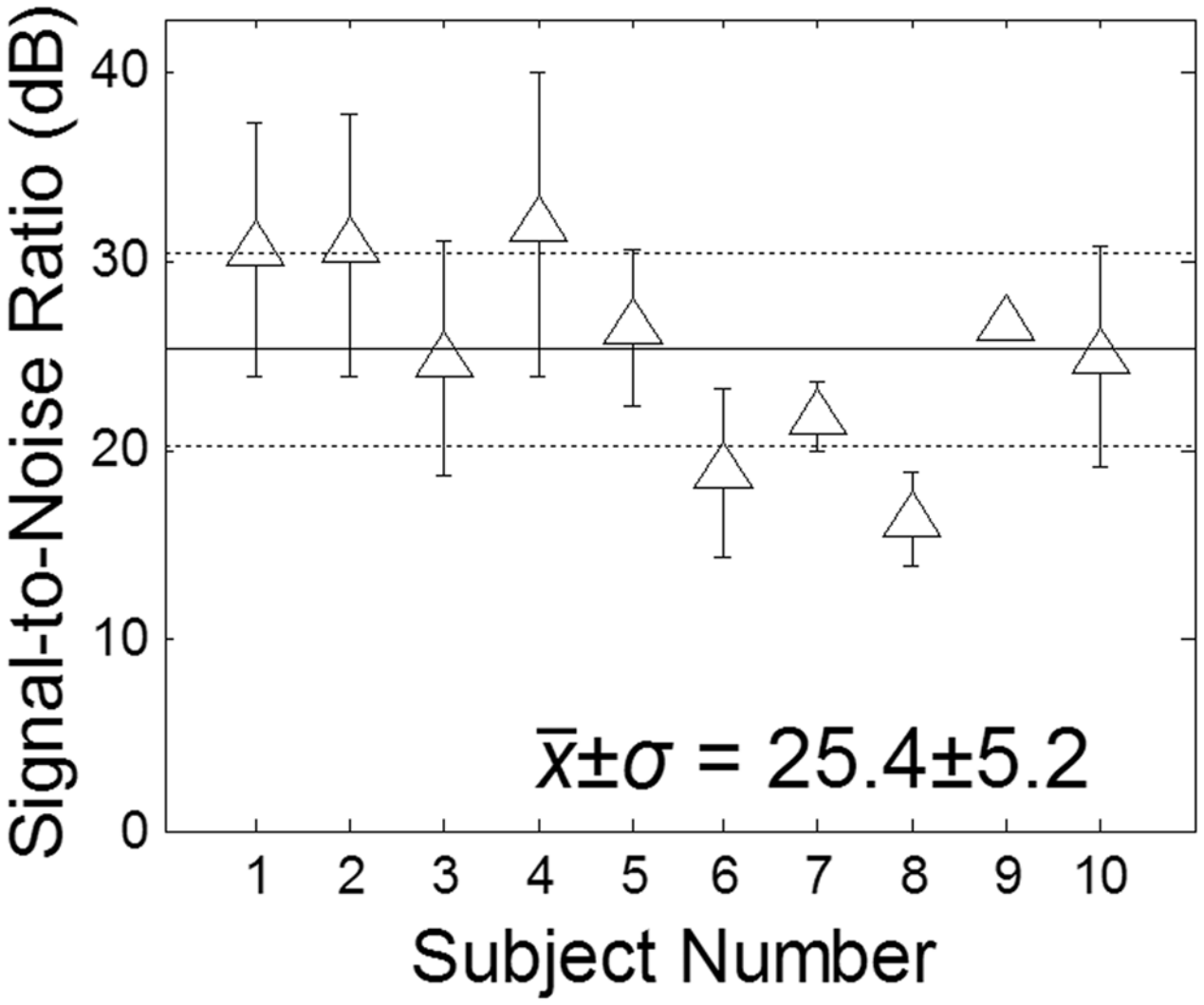

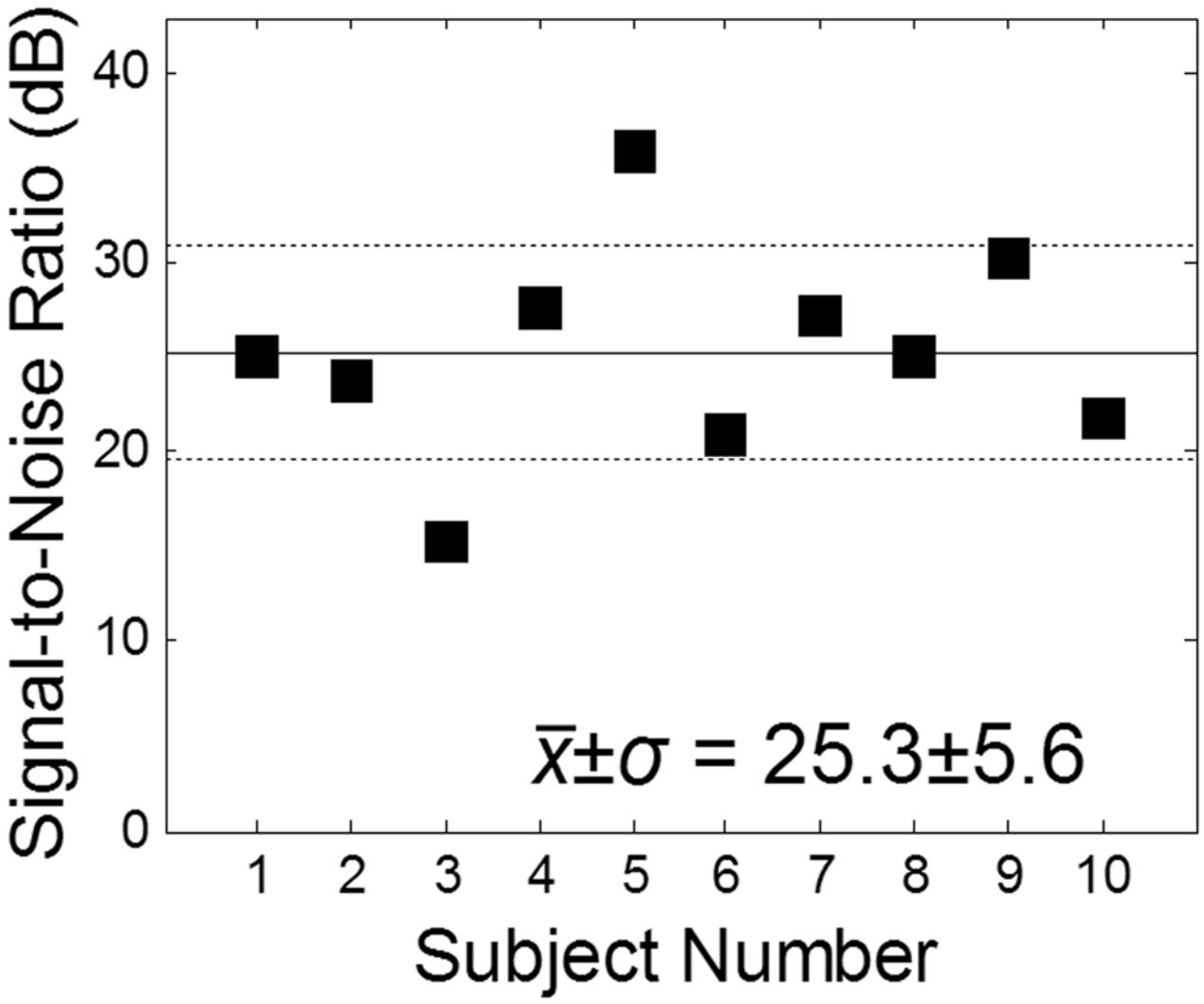

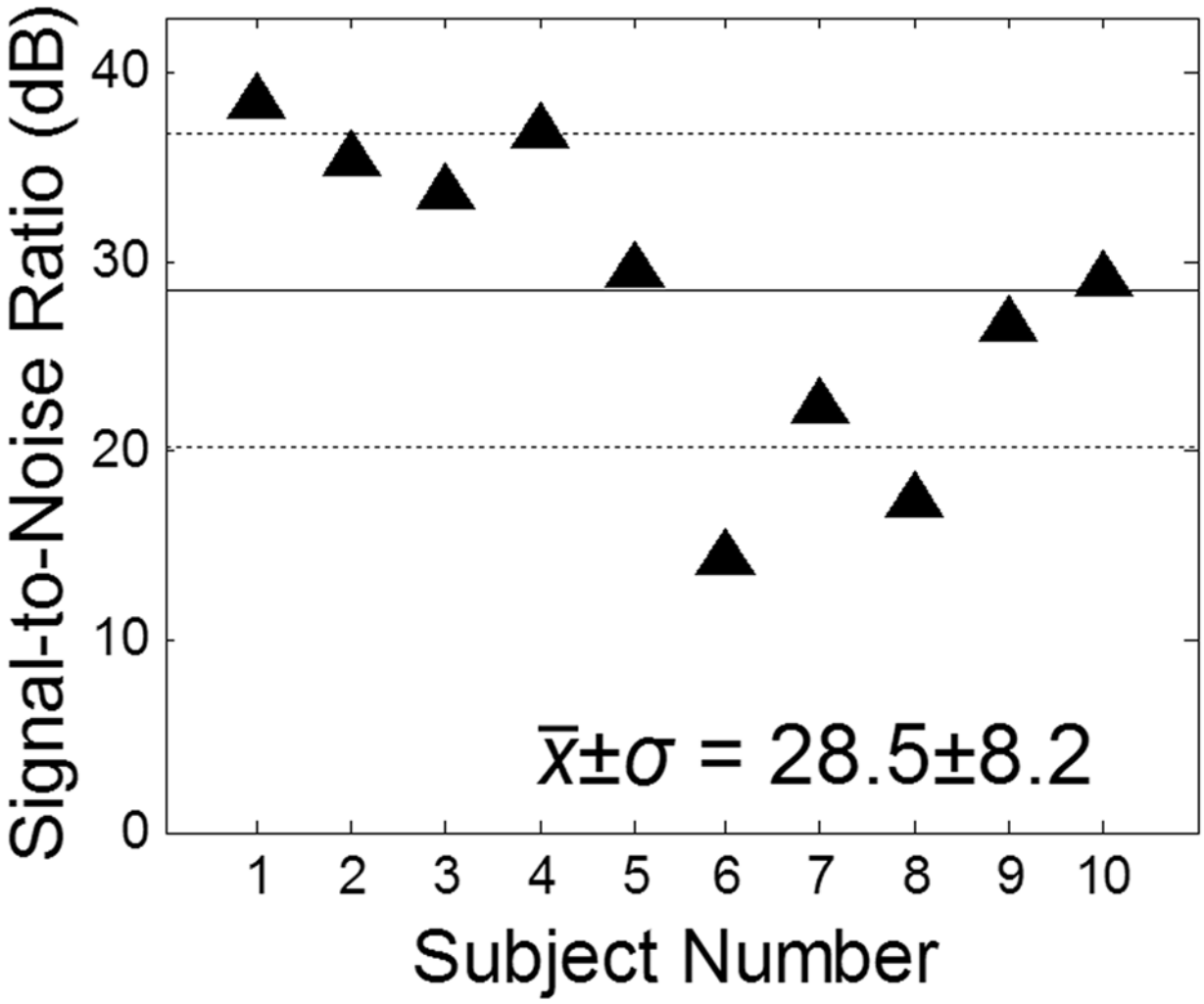

Figure 9.

Signal-to-noise ratios (SNR) for the identified signal peaks in both the MRI (**A** and **C**) and ITUM (**B** and **D**) data. (**A**,**B**) SNR for all identified signals peaks, (**C**,**D**) SNR for signal peaks as identified to originate from the ICSF. For (**A**, **B**, **C**, and **D**), solid line = mean value, dotted line = ±standard deviation, squares = MR data points, triangles = US data points, black squares or triangles = signal peaks originating from the ICSF, white squares or triangles = signal peaks originating from all other intracranial structures.